Journal of Materials Chemistry C

Accepted Manuscript

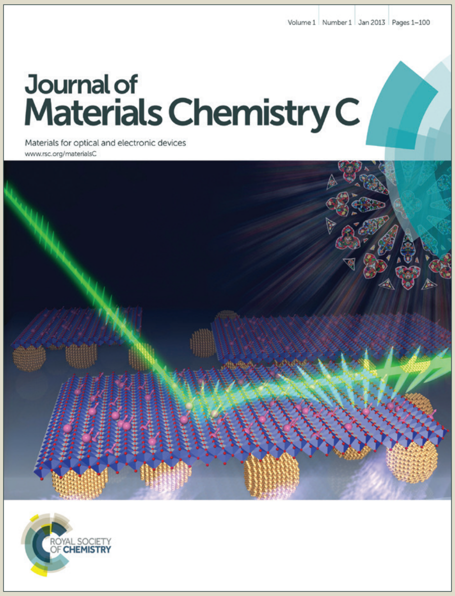

ROYAL SOCIETY OF CHEMISTRY

www.rsc.org/materialsC

Nonvolatile Memories Using the Electrets of Conjugated Rod-Coil Block Copolymer and Its Nanocomposite with Single Wall Carbon Nanotubes

*Yu-Cheng Chiu, Chien-Chung Shih, and Wen-Chang Chen**

Department of Chemical Engineering, National Taiwan University, Taipei, 10617 Taiwan

* To whom all correspondence should be addressed.

E-mail:chenwc@ntu.edu.tw (W.-C. Chen)

Abstract

We report high performance pentacene based organic field-effect transistor (OFET) memory devices using the electrets of conjugated rod-coil block copolymers, poly[2,7-(9,9-dihexylfluorene)]-*block*-poly(stearyl acrylate) (PF-*b*-PSA) and their nanocomposites with single-wall carbon nanotubes (SWCNT). The self-assembly PF-*b*-PSA electret with the PF nanorods covered by the crystalline PSA block exhibited a distinct hole-trapping capability due to the high electrical field generated in the confined dimension of the nanorods. Thus, it could effectively reduce the current leakage and stabilize data retention with a large memory window (35.8 V) and a high ON/OFF ratio ($>10^4$) over 10^4 s. Furthermore, the memory window of the device was further improved to 49.2 V by wrapping well-dispersed single-wall carbon nanotubes (SWCNT) in PF-*b*-PSA. The bundles of PF nanorods along the SWCNT effectively capture electrons and maintain similar retention characteristics as that of the PF-*b*-PSA device. This study demonstrated that the self-assembled conjugated rod-coil block copolymers and their nanocomposites could act as charge-storage electrets for high performance OFET memory devices through the precise morphology control.

KEYWORDS: rod-coil block copolymer, organic memory, polymer electret, carbon nanotube, nanocomposites.

1 Introduction

Organic field-effect transistor (OFET) type nonvolatile memories[1-8] have attracted extensive scientific interest due to their advantages of the non-destructive reading, multi-bit storage, and easily combined with circuits.[9-13] A typical configuration of OFET memory devices is a conventional transistor with an additional charge storage layer (named as the electret) between the semiconductor layer and dielectric layer. The electret is employed to create the hysteresis behavior and modulate high- and low-conducting state, including metallic nano-floating gate dielectrics,[14-17] organic ferroelectric oriented-dipole dielectric materials,[18-20] and polymer electrets.[21-26]

Among the studied electrets, the polymer-based electrets with the advantages of low cost and solution processability compared to the metallic nano-floating gate that require multi-procedures for preparing well-dispersed nanoparticles. The memory window, an index for the charge-storage capability, is strongly dependent on the hydrophobicity, conjugation length, and architecture of polymer electrets. For example, polymer electrets with hydroxyl groups exhibited much noticeable hysteresis by trapping electrons than that of the counterparts with non-polar molecules, such as polystyrene.[15,26,27] We recently showed that the memory window could be enlarged by enhancing the conjugation length of π-conjugated moieties of fluorene or thiophene or through the star-branched architecture of triphenylamine.[23,24,28,29]

Self-assembly nanostructures derived by amphiphilic block copolymers have been considered a candidate for electrets.[30,31] However, the commonly used block copolymers lack of effective charge trapping, such as poly(styrene-*b*-4-vinyl pyridine) micelles[32,33] and lamellar poly(styrene-*b*-*2*-vinyl pyridine) thin film.[16] Therefore, integrating metallic nanoparticles within the ordered periodic nanostructure were employed to produce a better trapping capability but the accompanied nanoparticle aggregates led to a small memory window or current leakage in their data retention.[16,32,33] More recently, we discovered the tunable memory characteristics using the maltoheptaose-*block*-polystyrene (MH-*b*-PS) electret by the morphological transfer from the random sphere, to vertical cylinders, and horizontal cylinders.[34] The memory window was further enhanced by the electret of MH(pyrene)-*b*-PS supramolecule due to the additional hole-trapping capability.

The employment of carbon-based materials, such as graphene, as nano-floating gate could have the charge storage and memory stability,[35] but it still remains a challenge to integrate those trapping segments into the device by solution processes. Single wall carbon nanotubes (SWCNT) also have been considered as promising carrier-transporting materials[36] and could well-disperse in conjugated materials through π-π interaction.[37] However, the OFET memory devices using the electrets of conjugated rod-coil copolymer and their nanocomposites with carbon-based materials have not been studied yet, as far as we know.

In this study, we demonstrate a simple and efficient strategy for manipulating the electrical characteristics of pentacene-based OFET using the electrets of conjugated rod-coil block copolymer, poly[2,7-(9,9-dihexylfluorene)]-*block*-poly(stearyl acrylate) (PF-*b*-PSA) and its nanocomposite with single carbon nanotubes (SWCNT). The self-assembled PF rod block is expected to trap the hole in the confined nanostructure while and PSA block acts as the tunneling layer. To the best of our knowledge, this is the first example of using conjugated rod-coil block copolymers as the charge-storage electrets in OFET memory devices. Furthermore, the well-dispersed SWCNT within the PF-*b*-PSA matrix further enhanced the electron-trapping capability for achieving a large memory window. As shown in Fig. 1, the pentacene-based OFET memory device incorporated with the block polymer electrets and fabricated with a bottom-gate/top-contact configuration. The effects of the materials morphology on the OFET memory characteristics were discussed in details.

2 Experimental Section

2.1 Materials. Polyfluorene macroinitiator (PF), PSA, and poly[2,7-(9,9-dihexylfluorene)]-*block*-poly(stearyl acrylate) (PF-*b*-PSA) were synthesized as reported previously.[38] The molecular weight (M_n) of PF, PF-*b*-PSA and PSA were 2610, 42280, and 27000, respectively, with the polydispersity indices (PDI) of 1.61, 1.57, and 1.38. Pentacene (sublimed) and single-walled carbon nanotubes (SWCNT) were obtained from Luminescence Technology Corp (Taiwan) from Strem Chemicals, Inc. (Massachusetts, USA), respectively, which were used as received. All of reagents or anhydrous solvents were commercially available and used as received.

2.2 Device fabrication. The devices were fabricated on highly doped n-type Si(100) wafer with a 100-nm-thick SiO_2 treated with a solvent cleaning procedure and dried under a steam of nitrogen. A homogenous toluene solution of synthetic polymer with concentration of 8 mg/ml was filtered through a PTFE membrane, and then spin-coated at 2000 rpm for 60 s onto the wafer substrate with 100-nm-thick SiO_2. The prepared thin films were allowed to dry in vacuum at 25 ^{0}C for 2 h. On the other hand, PF-*b*-PSA (12 mg) and SWCNT (3 mg) were suspended in toluene (3 ml) and ultra-sonicated for 90 min with a fixed temperature of 0^0C, and then centrifuged (Centrifuge 5424, Eppendorf) at 12000 g for 20 min. After removing the non-dispersed SWCNT precipitation, the black supernatant solution was spin-coated at 1200 rpm for 60 s onto same as above-mentioned substrate. The thickness of all studied electrets was controlled between 40 and

45 nm. Subsequently, the semiconducting layer, pentacene, was deposited with a growth rate of 0.5 nm s^{-1} at 10^{-7} torr. The top-contact source and drain electrodes were subsequently deposited by 100 nm thick gold through a regular shadow mask, and the channel length (L) and width (W) were 50 and 1000 μm, respectively.

2.3 Morphology Characterization. Atomic force microscopy (AFM) measurements were obtained with a Nanoscope 3D controller atomic force micrograph (AFM, Digital Instruments) operated in the tapping mode at room temperature was used to study the surface structure of pentacene and the studied electrets. Transmission electron microscope (TEM, JEOL 1230) was used to characterize by the internal morphology of the PF(SWCNT)-*b*-PSA electrets.

Measurements of Electrical Properties. All the measurements of the transistor memories were conducted using a Keithley 4200-SCS semiconductor parameter analyzer (Keithley Instruments Inc., Cleveland, OH, USA), with a Remote PreAmp (4200-PA) in a N_2-filled glove box at room temperature. Triaxial cables were connected into the probe station to minimize the background noise. The capacitance of the bilayer dielectrics was measured at 40 kHz on metal-insulator-metal (MIM) structures using a Keithley 4200-SCS instrument equipped with a digital capacitance meter (model 4210-CVU), similar to the method we reported previously.[24] The carrier mobility (μ) and threshold voltage (V_{th}) were estimated from slope and intercept of the linear plot of the square root of drain-to-source current ($I_{\mathrm{ds}}^{1/2}$) versus the gate voltage (V_{g}) by the following equation in the saturation regime:

$$I_{ds} = \frac{WC_{tot}\mu}{2L}(V_g - V_{th})^2 \quad (1)$$

where C_{tot} is the capacitance per unit area of total dielectric layer and V_{th} is threshold voltage.

3.1. Morphology of PF-*b*-PSA Thin Films

Fig. 2 shows the AFM images of PF, PF-*b*-PSA, and PSA thin films spin-cast from toluene solutions on SiO_2 substrate. As shown in the figure, PF and PSA thin films exhibit a relatively smooth surface with a low roughness of 0.31 and 0.94 nm, respectively. On the contrary, the PF-*b*-PSA film shows the anisotropic nanorod structure with the size of 53±9 nm in diameter and 188±24 nm in length. As reported previously,[23,38] the contact angles of a water droplet on SiO_2, PF, and PSA thin films were 530, 950, and 115^0, respectively. It indicates that both polymers do not prefer to cast on the 100-nm-thick SiO_2 specifically and thus the substrate effect on the above surface structure could be eliminated. As a result, the formation of a nanorod structure is probably driven by the immiscibility between the PF and PSA blocks, where the rigid chain conformation and strong π-π stacking of rigid PF backbones[39] results in the microphase separation from the PSA block.

The grazing incidence wide-angle X-ray scattering (GIXD) was used to characterize the molecular orientation and crystalline domain of the studied polymers. As shown in the insets of Fig. 2(a-c), the GIXD images of the as-cast PF thin film exhibits an amorphous structure while the PF-*b*-PSA and PSA ones show obvious peaks in the q_y direction. The corresponding *d*-spacing of 4.06 Å indicates the crystalline feature of the long-alkyl side chains on the PSA block, similar to that reported in the literature.[38] Furthermore, the PF conjugated block facilitates the formation of (100) diffraction spot along q_z axis and leads to a parallel lamellar packing of PF-*b*-PSA with the *d*-spacing of 2.92 nm, corresponding to the side-chain length of PSA.[40,41] The lattice spacing of PF-*b*-PSA thin film agrees with that of the bulk sample (Fig. S1(a) in ESI†).

These results suggest that the PF nanorods are horizontal in the PF-*b*-PSA film and the side chains of crystalline PSA are perpendicular to the substrate plane for minimizing the system entropy between hydrophobic PSA blocks and hydrophilic SiO_2, as illustrated in Fig. S1(b) (ESI†).

The grain sizes of pentacene on the electret surfaces of PF, PF-*b*-PSA, and PSA are in the same distribution of 170-250 nm due to the similar surface hydrophobicity between PF and PSA, as shown in the AFM images of Fig. S2 (ESI†). On the other hand, all of the X-ray diffraction patterns of pentacene shown in Fig. S3 (ESI†) exhibit similar crystalline peaks. The typical coexistence of two crystalline phases are "thin-film phase (001)" and "bulk phase (001')" diffraction peaks with vertical periodicity of 1.51 nm (q=0.417 Å^{-1}) and 1.44 nm (q=0.437 Å^{-1}) to polymeric substrates, where thin-film phase is the dominant phase with notable intensity since the deposited thickness of pentacene is thinner enough (< 50 nm) to suppress the formation of bulk phase, which could eliminate the carrier-transporting resistance produced by structural mismatch between these two crystalline phases.[42,43] Also, there is no significant change in the grain size and the intensity of the first-order peak (001) for all spectra, indicating the identity of pentacene crystallinity between the studied OFET devices.

3.2. OFET Memory Using PF-*b*-PSA Electrets

In general, the field-effect mobility (μ) of pentacene transistor with a typical p-type accumulation mode is highly dependent upon their grain size and crystal structure.[29,42,43] However, as the initial curves depicted in Fig. 3a, the studied OFET memory devices with PSA, PF, and PF-*b*-PSA reveal diverse mobilities of 0.58, 0.47 and 0.092 cm^2 V^{-1} s^{-1}, respectively, in the saturation region with high I_{On}/I_{Off} value of ~10^7. Note that the electrical characteristics listed in Table 1 were measured in dark to prevent the light-induced charge transfer or excitons.[44] Among them, the transfer curve of PSA device not only shows a poor hysteresis behavior between the forward and reverse scans but also exhibits the highest On current ~ 1.83x10^{-4}A at a fixed gate voltage of -50 V, implying the absence of the capture ability to the mobile carriers (holes) in the pentacene channel. On the contrary, the dual-sweep curves of the initial transfer characteristics of PF and PF-*b*-PSA show relatively lower on-currents and larger hysteresis phenomena with the positive-shifted threshold voltages (V_{th}) of backward sweeps of 31.3V (PF) and 37.5V (PF-*b*-PSA) (Fig. S4, ESI†), indicating the hole-trapping ability is successfully induced by incorporating the PF block into the electrets. However, the V_{th} of the backward sweep using PF-*b*-PSA shifts to a more positive region than that of PF device, attributed to the morphological effects that a higher electrical field generated in the cylindrically confined dimension[45,46] of the PF-*b*-PSA nanorods achieves a large hole-storage capability even at the low volume fraction of the PF block.

The transistor memories are extended from the regular transistors and operated by combination of the applied appropriate gate pulse to modulate the transfer curves, causing the diverse resistance at a fixed gate bias. As shown in Fig. 3(b), after the writing procedure of applying a gate pulse of +50 V for 1 s, the onset of transfer curves is maintained at the gate bias of 0~6 V and results in the written V_{th} of -6.86 V (PF) and -0.21 V (PF-*b*-PSA). The onset of the writing transfer curve in PF device is still close to 0 V as well as its initial sweep implies the lack of electron trapping owing to its electron-donating nature, while the slightly shift to the positive region of writing curve in PF-*b*-PSA device is probably owing to the electron trapping by tiny dipoles produced from the oxygen atoms in the side chains of PSA.[26,47] In the following, the transfer curves could be substantially switched to the negative direction with the threshold voltages of -35.7 V(PF) and -36.0 V(PF-*b*-PSA) after the erasing procedure of applying a gate pulse with -50 V for 1 s to trap the holes by the electron-donating polyfluorene in the studied electrets. Therefore, the memory windows (ΔV_{th}), the difference between the V_{th} shifts of the writing and erasing curves, of the PF and PF-*b*-PSA are 28.8V and 35.8 V, respectively.

More important, the long-term stability of the charges trapped within electrets is a key index for a nonvolatile OFET memory. Fig. 3(c) shows the ability to retain data with the retention time after the writing and erasing operations. The readout current value of the ON state at a fixed Vg of -10 V for PF device decreases linearly in the initial stage and then maintains at low current value of $4.7\mathrm{x}10^{-12}$ A over a monitoring time of 8000 s, presenting a poor retention characteristics due to the conjugated PF block in the electret causing the charge dissipates rapidly. On the sharp contrast, the ON current values monitored at 8000 s for the PF-*b*-PSA device is ameliorated significantly to $1.04\mathrm{x}10^{-8}$ A, leading to a better retention time longer than $1.2\mathrm{x}10^{4}$ s with a high ON/OFF ratio of $>10^{4}$. It indicates the advantages using self-assembled conjugated rod-coil block copolymer as the electret as described in the following: (i) high built-in electric field produced by low dielectric constant PSA tunneling layer that usefully maintains the charge injection ability from pentacene to the PF block under the writing and erasing gate pulses,[14,15,34] ii) discrete PF nanorods as trapping segments that effectively reduces the current leakage,[15-17,48] iii) crystalline comb-like PSA coil segments that could play an blocking layer to resist the de-trapping of store charges after removing the gate bias.[49] Note that the dielectric constant of PF, PF-*b*-PSA, and PSA estimated from the measured capacitance at the frequency of 40 kHz is 3.03, 2.59, and 2.37, which decreases with introducing non-polar PSA moiety.

3.3. Transistor Memories using the PF (SWCNT)-*b*-PSA Electret

Morphology of PF(SWCNT)-*b*-PSA Thin Film. Even though the enhanced hole-storage stability have been achieved by self-assembly rod-coil copolymers, the devices with the PF-*b*-PSA electret show a poorly electron-trapping capability after the writing operation due to the electron-donating nature of polyfluorene. By considering the extensive π-conjugated structures of the rod blocks, dispersing metallic SWCNT [36,37,50] in the electret is a feasible strategy to further enhance the electron injection for achieving a large memory window. In addition, the insulating PSA coil block could provide the de-bundled SWCNT with a good solubility and long-term stability in the suspension after centrifugation with 12,000 g for 20 min;[37] therefore, the color of the PF(SWCNT)-*b*-PSA suspension is blacker than that of PF(SWCNT), and the suspension is very stable without the precipitation after over a half year of storing at room temperature (Fig. S5, ESI†).

The thin film of PF(SWCNT)-*b*-PSA with the thickness of c.a. 44 nm were prepared from spin coating and characterized by AFM and TEM. As shown in Fig. 4(a), the PF nanorod structure becomes larger in length and width compared to PF-*b*-PSA (Fig. 2(b)), and becomes bundles of nanorods at specific points along the axis of SWCNT. Note that toluene is a common solvent for both polymer blocks of PF-*b*-PSA but a poor solvent for SWCNT. It suggests that the stronger χ (Flory-Huggins interaction parameter) value is induced once the strong π-π interaction formed between PF block and SWCNT, driving a significantly microphase separation in the prepared solution compared with the PF-*b*-PSA solution without SWCNT.[39] Also, the corresponding enlarged TEM images (Fig. 4b) with about $1\mu m^2$ without staining is used to confirm that the SWCNT with 6 nm in diameter indeed are dispersed within PF(SWCNT)-*b*-PSA electret. It indicates that SWCNT are surrounded by self-assembly PF nanorods since using AFM image does not show the SWCNT structure. In addition, PF(SWCNT)-*b*-PSA thin film also reveals the crystalline PSA property and the quenched photoluminescence spectra in comparison with pristine PF-*b*-PSA thin film (Fig. S1(c) and S6 in ESI†), indicating that lower work function of SWCNT could effectively capture the electrons form the photo-excited excitons,[51] i.e., charge transfer, due to the presence of PF(SWCNT) hybrids.

OFET Memory Performance using the PF(SWCNT)-*b*-PSA as Electret. The PF(SWCNT)-*b*-PSA thin film sandwiched between two conductors was first employed to measure the leakage currents in comparison with the thin films of PSA and PF-*b*-PSA in Fig. S7 (ESI†). Similar to the results of PSA and PF-*b*-PSA in a fixed range of the bias scan, the PF(SWCNT)-*b*-PSA electret exhibits a low leakage current density[52] of ~$3\mathrm{x}10^{-7}$ A/cm^2 since the PF(SWCNT) hybrids are effectively covered by the comb-like crystalline PSA block, which could avoid the SWCNT contacting with the electrodes or semiconducting layer in the OFET device directly.

The analog pentacene-based device incorporated with PF(SWCNT)-*b*-PSA as electret was prepared to explore the OFET memory behavior. As the metallic SWCNT possesses rich carrier-withdrawing capability, the field-effect mobility measured in the saturation region of PF(SWCNT)-*b*-PSA decreases to 0.005 $\mathrm{cm^2V^{-1}s^{-1}}$ even if the crystalline structure of pentacene in Fig. S3 (ESI†) is similar to the devices that do not contain the SWCNT in the electrets. However, the PF(SWCNT)-*b*-PSA device still maintains appreciable $I_{\mathrm{On}}/I_{\mathrm{Off}}$ of ~10^5 and p-type accumulation mode, suggesting no ambipolar behavior induced by the electrets. To investigate the electrical memory performance and compare with PF-*b*-PSA OFET memory, the writing and erasing processes were applied equally as aforementioned conditions. Fig. 4(c-d) and Table 1 shows the transfer characteristics of the PF(SWCNT)-*b*-PSA memory device. Fig. 4c presents a prominent hysteresis loop with 59.6 V hysteresis window defined by the difference of V_{th}

between forward (21.4 V) and backward sweeps (-38.2 V), indicating the incorporation of SWCNT into electret not only shows the electric bistability behavior but also improves the carrier-capturing ability.

In Fig. 4d, the V_{th} of the writing curve for PF(SWCNT)-*b*-PSA device is 20.55 V which exhibits an obviously shift to positive region compared with that of PF-*b*-PSA device (-0.21 V), exhibiting the induced electrons effectively inject into dispersed SWCNT. For the erasing process, the V_{th} is further switched to -28.7 V that maintains the hole-trapping polyfluorene rod as well as PF-*b*-PSA device. As a result, the memory window is significantly enlarged from 35.8 V (PF-*b*-PSA) to 49.2 V (PF(SWCNT)-*b*-PSA), more than 60% of the whole sweeping-voltage range, with the highest trapping density (Δn) of $7.06\text{x}10^{12}\text{cm}^{-2}$ that is comparable (or even better) to that of the state-of-the-art nano-floating gate and block copolymer-nanoparticle hybrid memory devices.

The retention capability of nonvolatile OFET memory devices was measured after the application of +50 V (ON state) and -50 V (OFF state) gate pulses for 1 s to investigate the carrier stability in PF(SWCNT)-*b*-PSA electret. As shown in Fig. 5a, the stability extracted at the zero gate-source voltage for the ON and OFF current states of PF(SWCNT)-*b*-PSA device could be kept at least longer than 10^4 s with the ON/OFF ratio over 10^4. This above results are attributed to not only the PF(SWCNT) hybrids for the holes/electrons capturing but also the crystalline PSA passivation layer that could restrain the trapped charges from penetrating into active layer when the gate pulse is removed. Also, the PF(SWCNT)-*b*-PSA device was tested by the cycle of the writing/reading/erasing/reading (WRER) operation to investigate the reproducible and reversible stability. As shown in Fig. 5(b-c), it shows a stable switching behavior with obvious ON/OFF states and displays an excellent reversibility between the writing and erasing states with a conductance change of ~10^3 over 200 cycles.

3.4. Proposed mechanism for PF(SWCNT)-PSA electrets

The memory performance of OFET memory based on PF(SWCNT)-*b*-PSA can be elucidated through the mechanism proposed in terms of energy level diagram in Fig. 6. The HOMO energy levels of pentacene[29,34] and low-molecular-weight polyfluorene[53] are -3.2, and -2.44 eV, respectively; while their LUMO levels are -5.0, and -5.39 eV. In addition, the work function of SWCNT is -4.3 eV[54] whereas PSA is an insulator. During the writing process, a large amount of electrons are induced in LUMO level of pentacene by the positive electric field and immediately tunnels to SWCNT through PSA (Fig. 6a), causing that the V_{th} of the writing curve substantially shifts to a positive direction owing to the extra holes accumulated in the active channel of pentacene before the V_g scans. This electron-trapping capability of SWCNT is coincident with the photoluminescence result in Fig. S6 (ESI†). As further applying a negative gat-source bias (erasing process), a large amount of electric-field induced holes are injected to the HOMO level of electron-donating polyfluorene, where not only occurs recombination with the electrons trapped in SWCNT but also captures the supplementary holes; therefore, the V_{th} of the erasing curve obviously moves to positive region and the device returns to a low-conductance state (OFF state) at the $V_g = 0$ V.

Also, using low dielectric constant polymer as tunneling layer benefits the trapping process on the metallic-based nano-floating gate memory has been demonstrated since the built-in field generated by tunneling layer is inverse proportion to the dielectric constant. In this study, the PSA block with dielectric constant of 2.37 that is much lower than wild-used PS or PMMA due to its long alkyl side chain groups. As a result, the low-k PSA matrix plays an important tunneling layer, where provides large built-in field to inject carriers into nano-floating charge-storage segments once applying the electric-induced holes/electrons in the semiconductor-electret interface. Furthermore, the crystalline nature of PSA block could facilitate to retain trapped charges within electrets when the gate-source bias is removed, resulting in superior retention characteristics.

4 Conclusions

We have demonstrated that the high performance OFET memory devices could be achieved using the nanostructured electrets derived from conjugated rod-coil block copolymer, PF-*b*-PSA and its nanocomposites with single wall carbon nanotube. Self-assembled PF rod block played an important role to improve hole-trapping capability, while the low dielectric constant PSA block provided high built-in electric field for effectively carrier injection. Furthermore, the well-separated SWCNT in PF-*b*-PSA were constructed by strong π-π interaction between polyfluorene and SWCNT, resulting in an enhanced memory window up to 49.2 V, stable retention time over 10^4 s with ON/OFF-current ratio ($>10^4$), and stable reversibility over 240 cycles. Our study showed that the conjugated rod-coil block copolymers and their nanocomposites could act as charge-storage electrets for high performance OFET memory devices.

Acknowledgements

We thank the financial support of this work from Ministry of Science and Technology, Taiwan.

References

1 P. Heremans, G. H. Gelinck, R. M. Muller, K. J. Baeg, D. Y. Kim and Y. Y. Noh, *Chem. Mater.*, 2011**, 23**, 341.

2 N. G. Kang, B. Cho, B. G. Kang, S. Song, T. Lee and J. S. Lee, *Adv. Mater.*, 2012, **24**, 385.

3 R. C. G. Naber, K. Asadi, P. W. M. Blom, D. M. de Leeuw and B. de Boer, *Adv. Mater.*, 2010, **22**, 933.

4 K.-J. Baeg, Y.-Y. Noh, J. Ghim, S.-J. Kang, H. Lee and D.-Y. Kim, *Adv. Mater.*, 2006, **18**, 3179.

5 C. A. Di, F. Zhang and D. Zhu, *Adv. Mater.*, 2013, **25**, 313.

6 S.-T. Han, Y. Zhou, Z.-X. Xu, L.-B. Huang, X.-B. Yang and V. A. L. Roy, *Adv. Mater.*, 2012, **24**, 3556.

7 S. J. Kim and J. S. Lee, *Nano Letter*, 2010, **10**, 2884.

8 Y. Guo, C. A. Di, S. Ye, X. Sun, J. Zheng, Y. Wen, W. Wu, G. Yu and Y. Liu, *Adv. Mater.*, 2009, **21**, 1954.

9 Q. D. Ling, D. J. Liaw, C. Zhu, D. S. H. Chan, E. T Kang and K. G. Neoh, *Prog. Polym. Sci.*, 2008, **33**, 917.

10 W. P. Lin , S. J. Liu, T. Gong, Q. Zhao and W. Huang, *Adv. Mater.*, 2014, **26**, 570.

11 S. K. Hwang, I. Bae, S. M. Cho, R. H. Kim, H. J. Jung and C. Park, *Adv. Funct. Mater.*, 2013, **23**, 5484.

12 J. I. Sohn, S. S. Choi, S. M. Morris, J. S. Bendall, H. J. Coles, W. K. Hong, G. Jo, T. Lee and M. E. Welland, *Nano Lett.*, 2010, **10**, 4316.

13 T. Sekitani, T. Yokota, U. Zschieschang, H. Klauk, S. Bauer, K. Takeuchi, M. Takamiya, T. Sakurai and T. Someya, *Science*, 2009, **326**, 1516.

14 K.-J. Baeg, Y.-Y. Noh, H. Sirringhaus and D.-Y. Kim, *Adv. Funct. Mater.*, 2010, **20**, 224.

15 M. Kang, K.-J. Baeg, D. Khim, Y.-Y. Noh and D.-Y. Kim, *Adv. Funct. Mater.*, 2013, **23**, 3503.

16 Q. Wei, Y. Lin, E. R. Anderson, A. L. Briseno, S. P. Gido and J. J. Watkins, *ACS Nano*, 2012, **6**, 1188.

17 S.-T. Han, Y. Zhou, C. Wang, L. He, W. Zhang and V. A. L. Roy, *Adv. Mater.*, 2013, **25**, 872.

18 S. J. Kang, Y. J. Park, I. Bae, K. J. Kim, H.-C. Kim, S. Bauer, E. L. Thomas and C. Park, *Adv. Funct. Mater.*, 2009, **19**, 2812.

19 R. Schroeder, L. A. Majewski and M. Grell, *Adv. Mater.*, 2004, **16**, 633.

20 R. C. G. Naber, C. Tanase, P. W. M. Blom, G. H. Gelinck, A. W. Marsman, F. J. Touwslager, S. Setayesh and D. M. Leeuw, *Nat. Mater.*, 2005, **4**, 243.

21 K. J. Baeg, Y. Y. Noh, J. Ghim, B. Lim and D. Y. Kim, *Adv. Funct. Mater.*, 2008, **18**, 3678.

22 Y. H. Chou, N. H. You, T. Kurosawa, W. Y. Lee, T. Higashihara, M. Ueda and W. C. Chen, *Macromolecules*, 2012, **45**, 6946.

23 J. C. Hsu, W. Y. Lee, H. C. Wu, K. Sugiyama, A. Hirao and W. C. Chen, *J. Mater. Chem.*, 2012, **22**, 5820.

24 Y. C. Chiu, C. L. Liu, W. Y. Lee, Y. Chen, T. Kakuchi and W. C. Chen, *NPG Asia Mater.*, 2013, **5**, e35.

25 W. Wu, H. Zhang, Y. Wang, S. Ye, Y. Guo, C. Di, G. Yu, D. Zhu and Y. Liu, *Adv. Funct. Mater.*, 2008, **18**, 2593.

26 T. D. Tsai, J. W. Chang, T. C. Wen and T. F. Guo, *Adv. Funct. Mater.*, 2013, **23**, 4206.

27 M. Egginger, M. I. Vladu, R. Schwödiauer, A. Tanda, I. Frischauf, S. Bauer and N. S. Sariciftci, *Adv. Mater.*, 2008, **20**, 1018.

28 Y. H. Chou, S. Takasugi, R. Goseki, T. Ishizone and W. C. Chen, *Polym. Chem.*, 2014, **5**, 1063.

29 Y. C. Chiu, T. Y. Chen, C. C. Chueh, H. Y. Chang, K. Sugiyama, Y. J. Sheng, A. Hirao and W. C. Chen, *J. Mater. Chem. C*, 2014, **2**, 1436.

30 Y. Mai and A. Eisenberg, *Chem. Soc. Rev.*, 2012, **41**, 5969.

31 C. L. Liu, C. H. Lin, C. C. Kuo, S. T. Lin and W. C. Chen, *Prog. Polym. Sci.*, 2011, **36**, 603.

32 C. M. Chen , C. M. Liu , K. H. Wei , U. S. Jeng and C. H. Su, *J. Mater. Chem.*, 2012 , **22** , 454.

33 W. L. Leong, P. S. Lee, A. Lohani, Y. M. Lam, T. Chen, S. Zhang, A. Dodabalapur and S. G. Mhaisalkar, *Adv. Mater.*, 2008, **20**, 2325.

34 Y. C. Chiu, I. Otsuka, S. Halila, R. Borsali and W. C. Chen, *Adv. Funct. Mater.*, 2014, **24**, 4240.

35 S. Bertolazzi, D. Krasnozhon and A. Kis, *ACS Nano*, 2013, **7**, 3246.

36 H. W. Lee, Y. Yoon, S. Park, J. H. Oh, S. Hong, L. S. Liyanage, H. Wang, S. Morishita, N. Patil, Y. J. Park, J. J. Park, A. Spakowitz, G. Galli, F. Gygi, P. H. S. Wong, J. B. H. Tok, J. M. Kim and Z. Bao, *Nat. Commun.*, 2011, **2**, 541.

37 J. Zou, L. Liu, H. Chen, S. I. Khondaker, R. D. McCullough, Q. Huo and L. Zhai, *Adv. Mater.*, 2008, **20**, 2055.

38 Y. C. Chiu, C. C. Kuo, C. J. Lin and W. C. Chen, *Soft Matter*, 2011, **7**, 9350.

39 S. T. Lin, Y. C. Tung and W. C. Chen, *J. Mater. Chem.*, 2008, **18**, 3985.

40 M. Atsushi, S. Junichi, Y. Hidekazu and O. Yoshihito, *Macromolecules*, 1994, **27**, 7695.

41 R. J. Kline, D. M. DeLongchamp, D. A. Fischer, E. K. Lin, L. J. Richter, M. L. Chabinyc, M. F. Toney, M. Heeney and I. McCulloch, *Macromolecules*, 2007, **40**, 7960.

42 H. Yang, S. H. Kim, S. Y. Yang, L. Yang and C. E. Park, *Adv. Mater.*, 2007, **19**, 2868.

43 H. L. Cheng, Y. S. Mai, W. Y. Chou, L. R. Chang and X. W. Liang, *Adv. Funct. Mater.*, 2007, **17**, 3639.

44 B. Park, P. Paoprasert, I. In, J. Zwickey, P. E. Colavita, R. J. Hamers, P. Gopalan and P. G. Evans, *Adv. Mater.*, 2007, **19**, 4353.

45 Y. H. Chou, W. Y. Lee and W. C. Chen, *Adv. Funct. Mater.*, 2012, **22**, 4352.

46 Y. Zhou, S. T. Han, Z. X. Xu and V. A. L. Roy, *Adv. Mater.*, 2012, **24**, 1247.

47 Th. B. Singh, N. Marjanović, G. J. Matt, N. S. Sariciftci and R. Schwödiauer, *Appl. Phys. Lett.*, 2004, **85**, 5409.

48 Y. H. Chou, Y. C. Chiu and W. C. Chen, *Chem. Commun.*, 2014, **50**, 3217.

49 R. P. Ortiz, A. Facchetti and T. J. Marks, *Chem. Rev.*, 2010, **110**, 205.

50 M. S. Arnold, A. A. Green, J. F. Hulvat, S. I. Stupp and M. C. Hersam, *Nat. Nanotechnol.*, 2006, **1**, 60.

51 C. Li, Y. Chen, Y. Wang, Z. Iqbal, M. Chhowalla and S. Mitra, *J. Mater. Chem.*, 2007, **17**, 2406.

52 G. Xia, S. Wang, X. Zhao and L. Zhou, *J. Mater. Chem. C*, 2013, **1**, 3291.

53 W. C. Wu, C. L. Liu and W. C. Chen, *Polymer*, 2006, **47**, 527.

54 S. J. Kang, Y. Song, Y. Yi, W. M. Choi, S. M. Yoon and J. Y. Choi, *Carbon*, 2010, **48**, 520.

Table 1. The electrical and memory performance of the studied OFET memories using various polymer electrets.

	μ_{ave} [cm^{2}V^{-1}s^{-1}]	$I_{\mathrm{On}}/I_{\mathrm{Off,}}$ ave	$V_{\mathrm{th,\ ave}}$ of initial [V]	$V_{\mathrm{th,\ ave}}$ [V]		Memory window [V]	Trapping density Δn [cm^{-2}]
				Writing	**Erasing**		
PSA	0.58±0.04	5.7x10^{7}	-5.42	Negligible	Negligible	Negligible	Negligible
PF	0.47±0.05	4.6x10^{7}	-3.56	-6.86±1.1	35.7±4.1	28.8	4.06x10^{12}
PF-*b*-PSA	0.092±0.01	1.3x10^{7}	-3.40	-0.21±0.6	-36.0±1.5	35.8	4.77x10^{12}
PF(SWCNTs)-*b*-PSA	0.005±0.01	5.5x10^{5}	-1.93	20.55±2.3	-28.7±1.8	49.2	7.06x10^{12}

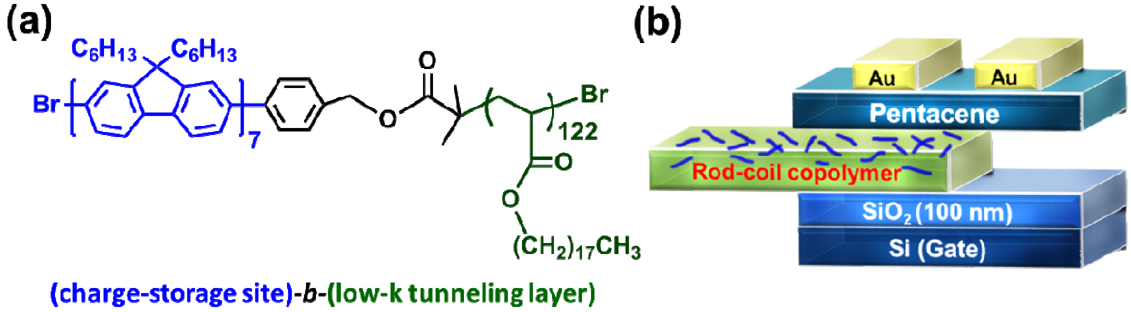

Fig. 1 (a) Chemical structure of PF-*b*-PSA, (b) schematic configuration of the pentacene-based OFET memory device.

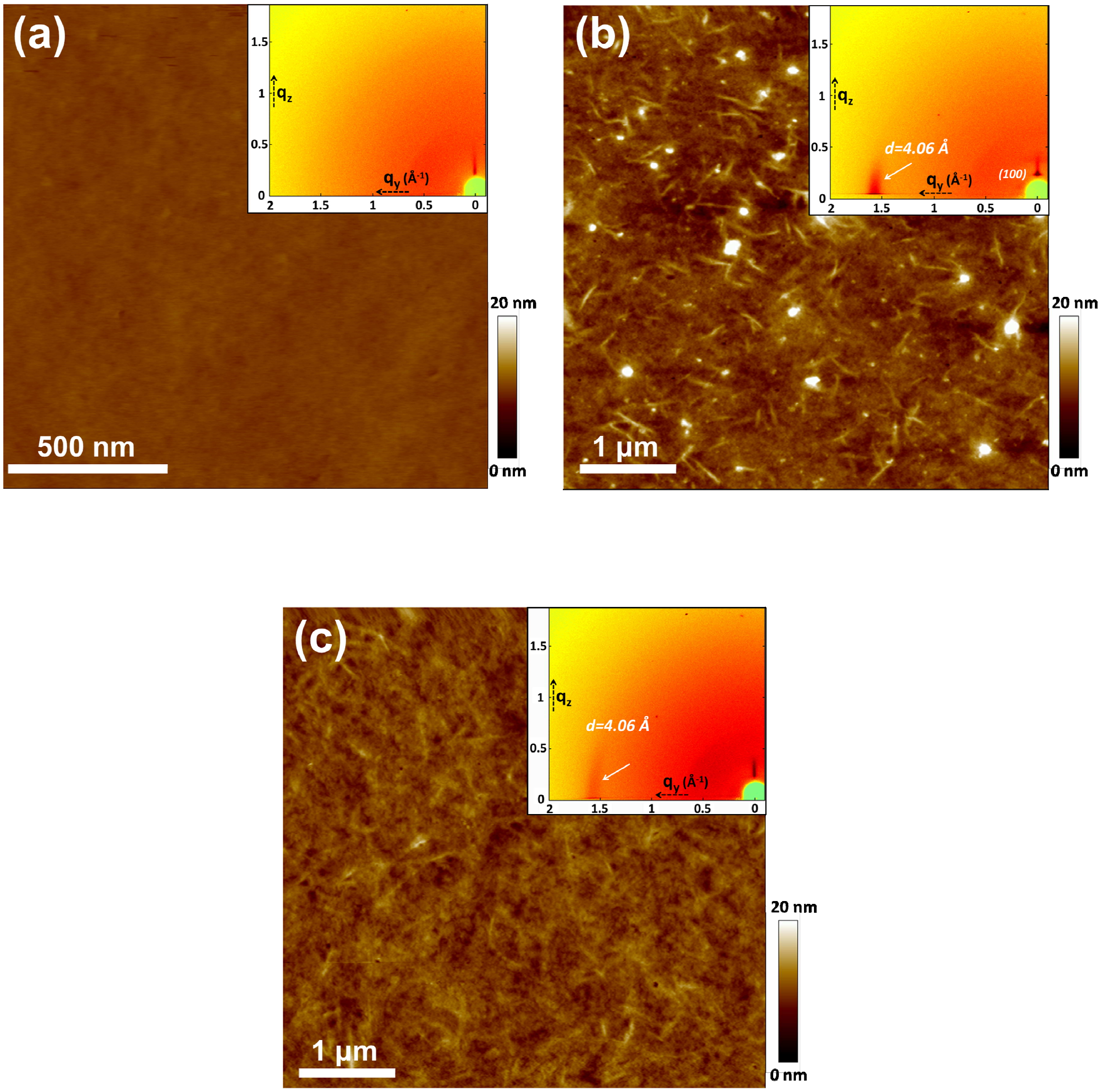

Fig. 2 The AFM height images of (a) PF, (b) PF-*b*-PSA, and (c) PSA films, ~40 nm in thickness. The insets of (a-c) are their corresponding 2D-GIXD images.

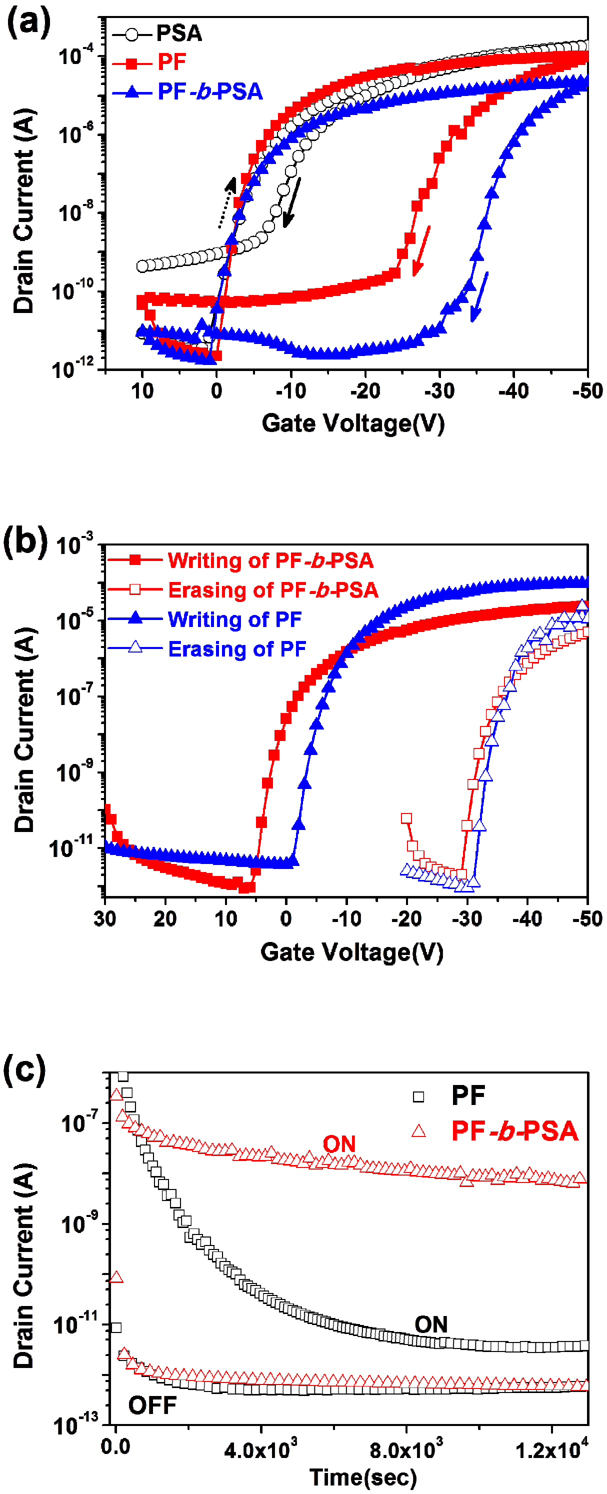

Fig. 3 (a) Initial transfer curves, (b) writing/erasing plots, and (c) the corresponding memory retention characteristics of the devices using PSA, PF, and PF-*b*-PSA as electrets at V_d= -30V.

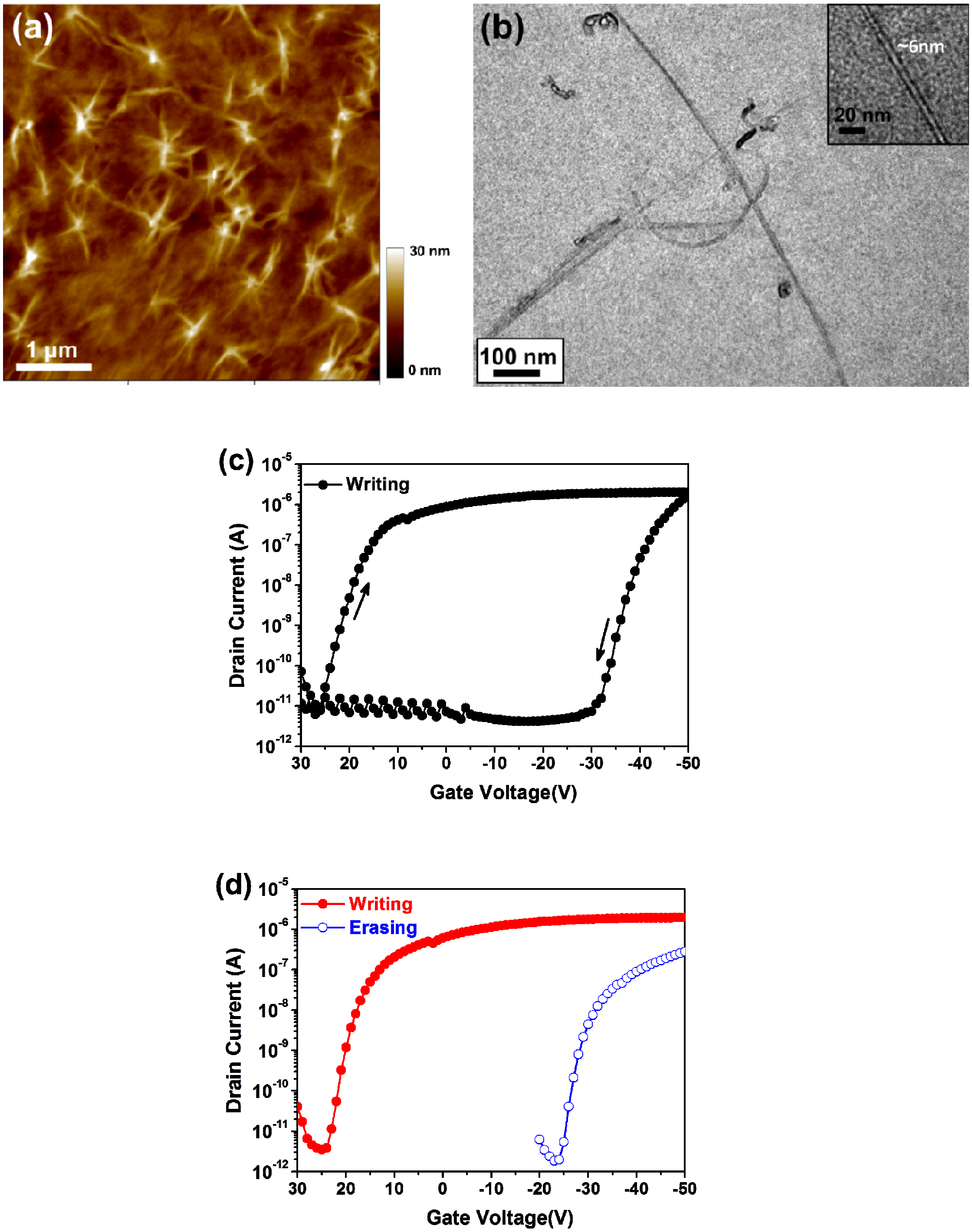

Fig. 4 (a)AFM height image and (b) TEM image of PF(SWCNT)-*b*-PSA thin film with thickness of ~43 nm. (c) Dual gate voltage sweeps after writing process (50 V, 1s) and (d) their transfer curves of the OFET memory device using PF(SWCNT)-*b*-PSA as the electret.

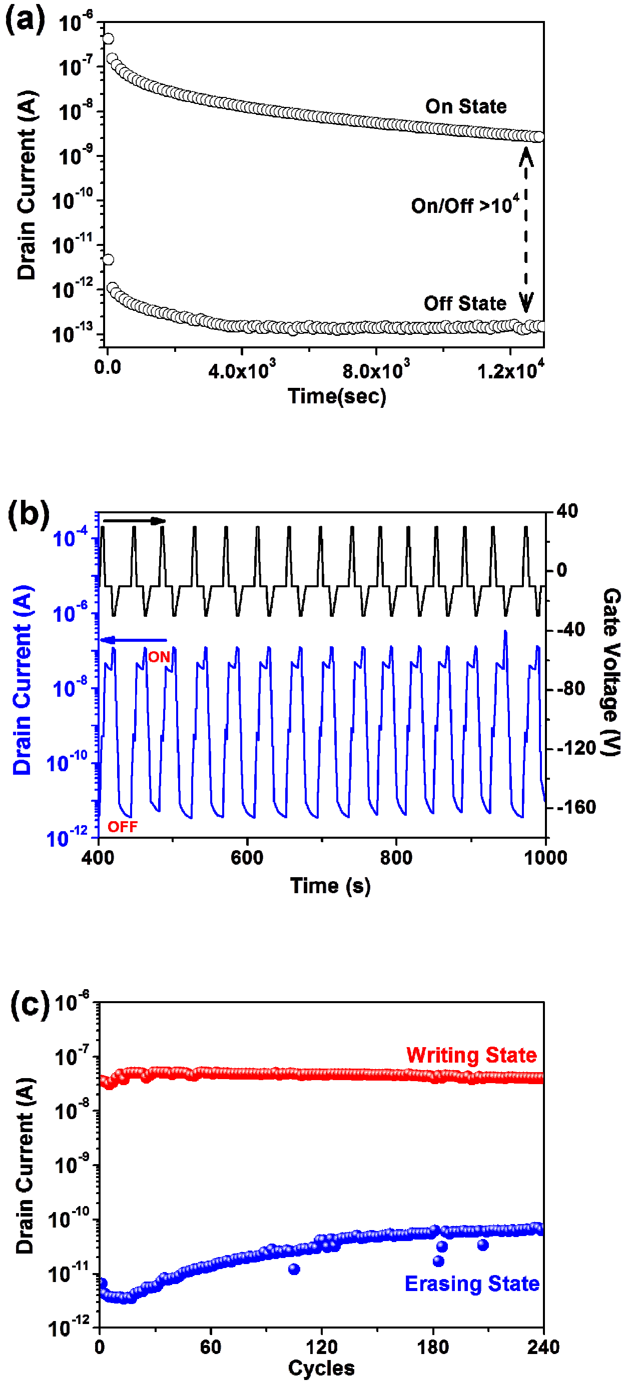

Fig. 5 (a) Memory retention characteristics after the writing and erasing operation on the OFET memory device with PF(SWCNT)-*b*-PSA as electret. The currents at ON and OFF states were read at V_g = -10V and V_d = -30V. (b) The reversible switching on the ON- and OFF- states and (c) the endurance characteristics of the device using PF(SWCNT)-*b*-PSA electret.

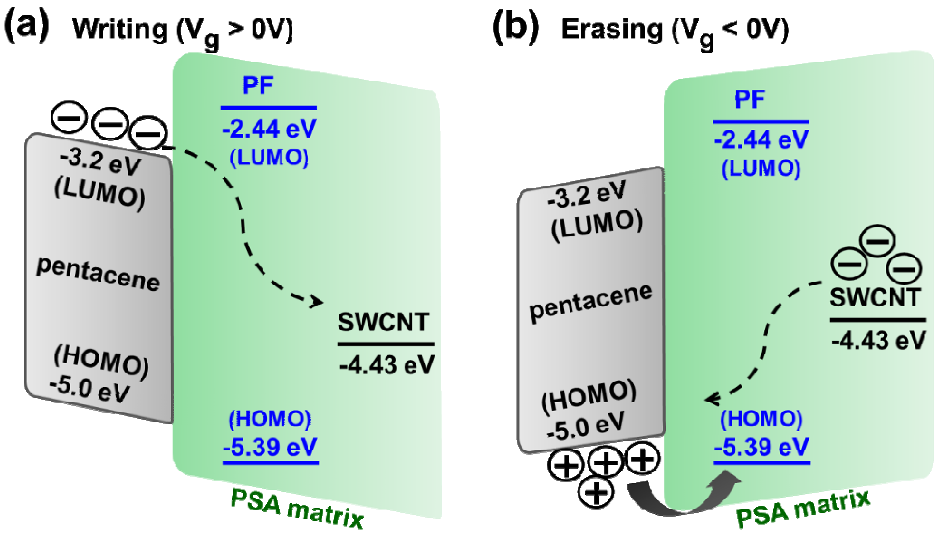

Fig. 6 Proposed mechanisms and energy band diagrams under the (a) positive and (b) negative bias for the OFET memory using PF(SWCNT)-*b*-PSA as electrets.

The table of contents entry:

Nonvolatile Memories Using the Electrets of Conjugated Rod-Coil Block Copolymer and Its Nanocomposites with Single Wall Carbon Nanotubes

By Yu-Cheng Chiu, Chien-Chung Shih, and Wen-Chang Chen*

Self-assembly conjugated rod-coil block copolymer and its nanocomposites with SWCNT could be used as the charge storage layer for high-performance OFET memory devices.